Proceedings of ISFOG 2025
5TH INTERNATIONAL SYMPOSIUM ON
FRONTIERS IN OFFSHORE GEOTECHNICS
Nantes, France | June 9-13 2025

ISBN 978-2-85782-758-0

Dynamic responses of monopile-supported DTU 10MW offshore wind turbine subjected to wind, wave and seismic loads

*K. Dib
Saint-Joseph University, Beirut, Lebanon

Ph. Alkhoury
Formerly Nantes University, Ecole Centrale Nantes, CRNS, GeM, UMR 6138 F-44600 Saint Nazaire, France

A.-H. Soubra
Nantes University, Ecole Centrale Nantes, CRNS, GeM, UMR 6138 F-44600 Saint Nazaire, France

F. Kaddah
Saint-Joseph University, Beirut, Lebanon

*kassem.dib@net.usj.edu.lb/ Kassem.Dib@univ-nantes.fr

ABSTRACT: Multi-megawatt monopile-supported Offshore Wind Turbines (OWTs) are widely adopted to efficiently extract the steady offshore wind energy. They are dynamically-sensitive structures to excitations and their foundations need to be designed with special concern for cyclic/dynamic loading. In this regard, three-dimensional (3D) non-linear (NL) finite element (FE) dynamic analyses are becoming crucial to analyze the behavior of OWTs making use of advanced soil constitutive models. The aim of this paper is to study the NL dynamic behavior of a large diameter monopile-supported DTU-10 MW OWT installed in dense sand and subjected to the combined effect of wind, wave and seismic loads. A detailed 3D FE model developed within Abaqus/Standard software was used in the analysis. This model considers the real geometrical configuration of the OWT superstructure and monopile foundation. It also considers the monopile-sand interaction and makes use of advanced soil constitutive models. Two soil constitutive models [SANISAND (SS) and HYPOPLASTIC (HP)] calibrated on the same Karlsruhe sand were adopted. Nonlinear 200s time-domain dynamic simulations were performed within Abaqus software under stochastically simulated scenarios of wind and wave loadings along with the Alkion earthquake applied at bedrock. Structural and geotechnical responses of the OWT as predicted using the two calibrated soil constitutive models were analyzed and compared. The numerical results have shown that the structure exhibited approximately the same response at mudline in the absence of earthquake loading, and greater displacements and rotations in presence of that loading when the HP soil model was used compared to the SS model. It was also shown that higher accelerations were observed in fore-aft and vertical directions at tower top during earthquake when the SS model was adopted compared to the HP model.

Keywords: Offshore wind turbine; Nonlinear dynamic analysis; Soil-structure interaction; Advanced soil constitutive models; Earthquake loading.

1 INTRODUCTION

Offshore wind turbines (OWTs) are becoming one of the most important and reliable sources of clean energy around the world. However, their sensitivity to environmental loads makes their structural design crucial and conservative. This paper focuses on the study of monopile-supported OWTs. In engineering practice, simplified models are often used for the analysis and design of such structures, employing beam elements for the superstructure, lumped mass to represent the rotor-nacelle assembly (RNA) at the top of the tower, and a Winkler beam model to simulate the soil-monopile foundation interaction [e.g. API (2011)]. Furthermore, the environmental loads are applied *via* static or sinusoidal cyclic loads. These methods cannot accurately predict the whole dynamic behavior of the OWT structure. Additionally, they are unable to account for the soil stiffness degradation with time under the dynamic/cyclic loads. On the other hand, limited studies have been documented in the scientific literature: some authors conducted an accurate model of the superstructure and a simplified one for the soil-structure interaction, while others focused on a rigorous modeling of the soil-monopile

system with a simplified model of the superstructure. For instance, Zuo et al. (2019) studied the dynamic response of a 5MW offshore wind turbine in the presence of wind, wave and earthquake loadings. In their study, although the OWT superstructure was explicitly modeled and the loads were defined stochastically, the soil-structure interaction was addressed using the simplified Winkler model. Eslami and Ghorbani (2022) studied the response of an OWT in a liquefied soil. In their study, the advanced SaniSand (SS) soil model developed by Dafalias and Manzari (2004) was adopted. However, the OWT superstructure and the environmental loads were addressed in a simplified manner.

An accurate analysis of the dynamic behavior of a monopile-supported OWT under different types of dynamic environmental loads necessitates a quite rigourous modelling of both the superstructure (including the RNA) and the soil-foundation interaction. FE analysis combined with an advanced soil constitutive model is currently the most effective method for examining the dynamic behaviour of an OWT. In this regard, Alkhoury et al. (2022) conducted a full 3D FE model of a monopile-supported DTU 10MW OWT embedded in sand using Abaqus/standard software where the superstructure (including the RNA) and the monopile foundation were modeled explicitly. Furthermore, these authors made use of the advanced SS and HP soil constitutive models. Nonlinear 10-minutes dynamic simulations were carried out in the presence of stochastically simulated wind and wave loads. However, seismic loads were not considered.

Following the work of Alkhoury et al. (2022), a 3D FE modelling is further applied herein to investigate the structural and geotechnical dynamic responses of the DTU 10MW OWT installed in dense sand and subjected to the combined actions of wind, wave and earthquake loadings. 200s nonlinear dynamic time-domain simulations were performed by applying the critical-state elasto-plastic soil constitutive model SS by Dafalias and Manzari (2004) and the HP soil model given by Wolffersdorff (1996) and further extended for the intergranular strain (IS) approach by Niemunis and Herle (1997). The purpose of employing two different advanced soil constitutive models was to compare the OWT responses as predicted by each model for the same sand. It should be noted here that the parameters of the Karlsruhe sand as adopted in this paper for both soil constitutive models are available on (Wichtmann.T web site) and they were obtained by calibration with laboratory experimental tests. Finally, it is important to note that the Sanisand and the hypoplastic model with intergrannular strain are both advanced soil constitutive models used to describe the behavior of granular materials such as sand under cyclic loading, but they differ in their formulation and assumptions. Sanisand is an advanced elasto-plastic model that incorporates critical state theory and dilatancy. The model includes a yield surface that defines the boundary between elastic and plastic behavior and a rotational hardening law to describe the evolution of the yield surface as the material deforms. The ultimate behavior of sand under large strains is essentially captured using the critical state theory. The model accounts as well for dilatancy by including a mechanism that allows the material to transition from dilative to contractive behavior depending on the stress state and the strain path. On the other hand, unlike traditional elasto-plastic models, the hypoplastic model does not rely on yield surfaces; instead, it is based on a hypoplasticty framework with a set of state variables evolving with loading which allows for a continuous stress rate-strain rate relation. Similar to the SS model, the HP captures the stress-dependent stiffness but with a focus on intergranular strains. Notice finally that the HP do not explicitly focus on dilatancy but can capture related behaviours through the intergranular strain concept. Both soil constitutive models are available as user-defined material UMAT libraries at the SoilModels website.

2 THREE-DIMENSIONAL FINITE ELEMENT MODEL

This section summarizes the finite element model used in this paper. As mentioned before, the 3D FE model used herein follows mainly the work of Alkhoury et al. (2022) but takes into account the seismic loads. Only a brief description of the 3D FE model of the OWT is provided herein. A complete and detailed description of this model may be found in Alkhoury et al. (2022).

Figure 1 shows the whole 3D model of the OWT (DTU-10 MW) developed within Abaqus software. As shown in this figure, the developed FE model consists of six main parts: (i) 3D soil domain, (ii) monopile having a diameter of 8.3 m and a total length of 65m, (iii) transition piece, (iv) turbine tower, (v) rotor/nacelle assembly, and (vi) blades.

In the 3D model, shell elements (S4 in Abaqus) were used to discretize the steel structure of the tower and the transition piece, while solid elements were used to discretize the steel monopile. The steel was considered as a linear elastic isotropic material. Secondary structural steel and equipment masses as well as the added mass effect (due to the surrounding water) were included in the 3D model by increasing the effective density of the steel.

Concerning the rotor/nacelle assembly, a reference point (RP) eccentric to the tower top and which coincides with the nacelle center of mass position was used to model the rotor/nacelle assembly as a lumped mass (point mass in Abaqus). The mass and the rotary inertia of the rotor/nacelle assembly were defined at this RP.

To accurately take into account the influence of the blades stiffness and geometry on the OWT dynamic response, each blade was divided along its length into 51 segments. A generalized beam cross-section was defined for every segment of the partitioned blade and for each cross-section, its corresponding stiffness and mass properties were assigned. Finally, a hinge connector was used to simulate the rotation of the blades with respect to the tower.

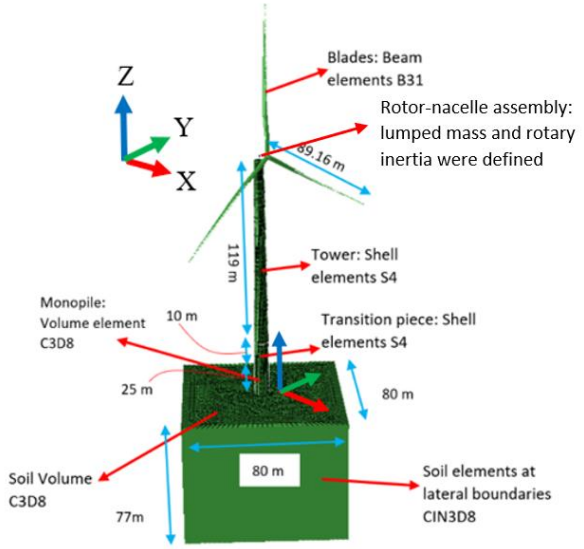

Figure 1. 3D model of the soil-OWT system

A 3D soil domain whose dimensions (80 m x 80 m x 77 m) was adopted. It was represented with hexahedral elements of type C3D8. The soil domain dimensions and mesh size were determined based on a sensitivity analysis taking into consideration the maximum allowable mesh size for earthquake load conditions as used by Kuhlemeyer and Lysmer (1973) and which is given as:

$$\Delta l = \left(\frac{1}{8} \sim \frac{1}{10}\right) \frac{V}{f_{max}} \qquad (1)$$

where Δl (m) is the maximum mesh size, V (m/s) is the shear wave velocity, and f_{max} (Hz) is the cut-off frequency that depends on the used seismic record. In this paper, the adopted values of V and f_{max} were respectively 139m/s and 2.7 Hz. Infinite elements (CIN3D8) in Abaqus were used for the lateral boundaries of the 3D soil domain. The purpose of these infinite boundaries is to prevent the reflection of the seismic waves back to the soil medium. Regarding the bottom boundary of the soil domain, both the horizontal and vertical displacements were restrained in the absence of the seismic load. In the presence of the seismic load, the bottom of the soil medium was subjected to the Alkion earthquake displacement time history. The small sliding, surface-to-surface and master/slave contact pair formulation implemented in Abaqus was used to model the contact interaction between the inner/outer surfaces of the monopile (master surfaces) and the surfaces of the soil (slave surfaces) outside and inside the monopile and at the bottom face of this monopile. The classical Coulomb friction model was used to describe the frictional behavior between the soil and the monopile. The interface friction coefficient of steel-saturated sand represents the tangent of the two-third of the friction angle of the saturated sand which typically ranges between 0.4 and 0.6 depending on the relative density of the sand. An interface friction coefficient of 0.4 was considered as in Alkhoury et al. (2022).

2.1 Soil parameters of the SS and HP constitutive models

This paper makes use of the SS (version 2004) and the HP with intergranular strain constitutive models to describe the soil behavior under dynamic loads. In all the dynamic simulations performed in this paper, a homogeneous soil medium made of Karlsruhe sand is selected. The parameters of the Karlsruhe sand for both constitutive models are available in (Wichtmann.T web site) as well as in Alkhoury (2022).

An initial void ratio of 0.77 corresponding to a dense sand with a relative density of 75% was used for both soil models. In this study, the impact of excess pore water pressure build-up on the soil shear stiffness degradation was not considered, the degradation was assumed to result solely from cyclic shear stresses induced by wind, wave and seismic loadings. Future studies are desirable to investigate the effect of excess pore water pressure buildup in dense sand on the responses of the OWT.

2.2 Damping

Damping of the OWT is modelled in Abaqus by means of material Rayleigh damping. In this paper, it was calculated for the case of an operational OWT by considering the total damping ratio as given in Alkhoury et al. (2022) in the fore-aft direction. It has a value of 3.93% for the rotating blades and a value of 1.12% for the tower. Notice that, no additional soil hysteretic damping was assumed in this analysis, as it

was considered only through the soil constitutive model equation.

2.3 Loading

The OWT dynamic responses were studied in this paper using the loading scenario LC10 from the UpWind project where the mean wind speed at hub height is between the cut-in and the cut-out speed of the DTU 10 MW. LC10 represents the design load case (DLC) 1.2 Power Production given by IEC 61400-1. In this load case, the 10-minutes mean wind speed at the hub height is 20 m/s, the significant wave height is equal to 2.76 m and the peak spectral period is equal to 6.99s. The aerodynamic loads along the tower and the blade and the hydrodynamic loads acting along the monopile in water were stochastically simulated based on the Kaimal spectrum for wind and JONSWAP spectrum for waves. The generation details are omitted herein for brevity. Regarding the seismic load, the Alkion earthquake recording in the three directions was adopted in this study and it was applied at the bottom boundary of the 3D soil domain. Figure 2 depicts the three components of the Alkion earthquake time history displacement recorded in rocky site (University of Cyprus-Website).

3 CALCULATION PROCEDURE AND RESULTS

The analysis steps of the different dynamic simulations may be described as follows:

- Geostatic step: Vertical and lateral soil stresses at rest are generated.
- Static step: The weight of the structure is applied to the soil medium.
- Pre-earthquake step: In this phase, only wind and wave loadings are applied with a duration of 100s.
- Earthquake application step: In this phase, a three-directional time history displacement was imposed at the base of the soil domain, along with wind and wave loads for a duration of 42s.
- Post-earthquake step: In this phase, only the wind and wave loadings continue to act on the OWT for a duration of 58s.

Calculations were conducted on INTEL® XEON® E5-2630 v3 server for a total simulation time of 200s. The results will be firstly delivered for the lateral displacements and rotations of the monopile at mudline, and then for the lateral and vertical accelerations at tower top.

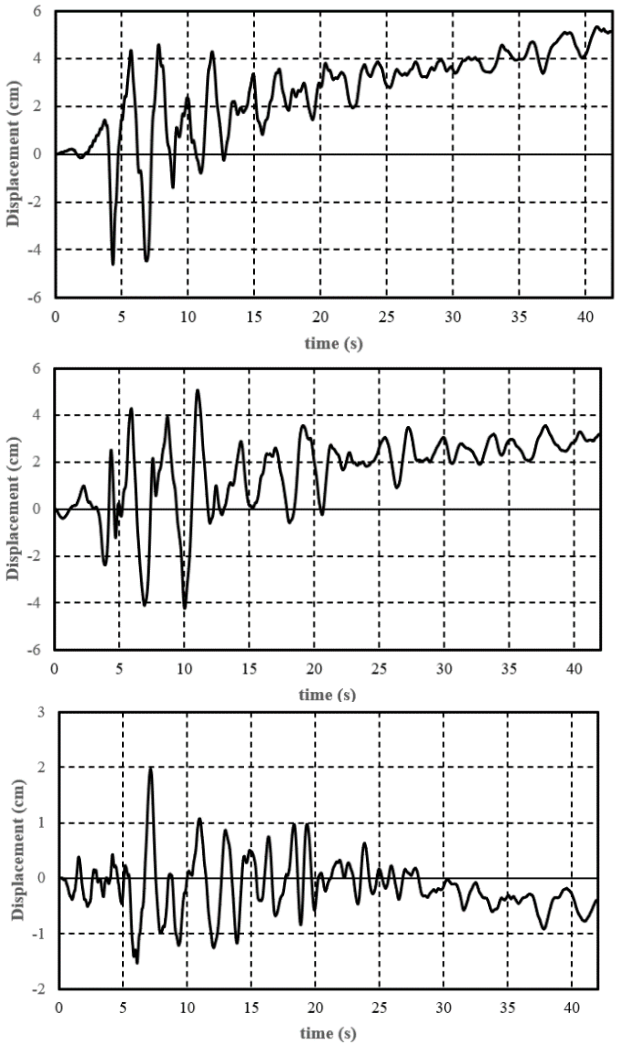

Figure 2. X, Y and Z components for Alkion earthquake displacement time history (from above to below).

3.1. Monopile lateral displacements and rotations at mudline

Figures 3-4 provide the monopile fore-aft and side-to-side displacements at mudline and Figures 5-6 provide the corresponding monopile rotations. Moreover, Figures 7-9 illustrate the shear stress-shear strain behavior during the pre-earthquake, the earthquake and the post-earthquake stages, at a point located 10 meters below the mudline and 10 meters away in the x-direction from the monopile. These figures will be discussed in the following three sub-sections according to the three stages. It is important to note that the monopile displacements time-histories at mudline are obtained by substraction of the total displacement calculated by the software at this level and the time history displacement applied at the bottom of the soil medium (bedrock).

3.1.1 Pre-earthquake stage

Figures 3-6 clearly show that the displacements and rotations of the pile at mudline are nearly identical for both soil models during the first 25 seconds of this stage. After this period, the displacements and rotations begin to diverge, with the SS model exhibiting slightly higher maximum values (Figures 3 and 5) than the HP model.

Figure 7 further demonstrates that both soil models display nearly identical stiffnesses, as indicated by the parallel green dashed line for SS and the blue dashed line for HP, both with similar slopes. Furthermore, this figure shows that the SS model exhibits an increase in plastic shear strain with each cycle, while the hypoplastic model (HP) exhibits almost no plastic strain between cycles.

As a conclusion, during the pre-earthquake stage where only wind and wave loads are applied, both soil models demonstrate nearly identical stiffnesses with no degradation. However, the SS model shows elasto-plastic behavior, while the HP model behaves almost elastically.

3.1.2 Earthquake stage

At this stage, the maximal fore-aft displacement of the monopile at mudline (Figure 3) is 62% higher for the HP model compared to that of the SS model, with values of 11.5 cm for HP and 7.1 cm for SS. In the side-to-side direction (Figure 4), the HP model shows a maximal displacement of 8.4 cm, which is 42% greater than that of the SS model (5.9 cm).

The fore-aft and side-to-side displacements observations align with the corresponding rotations. Indeed, Figure 5 illustrates that during the earthquake, the maximum fore-aft rotation (due to the combined wind, wave, and seismic loads) reaches 0.19° for the HP model which is 46% greater than that of the SS model with a maximum value of 0.13°. Similarly, the monopile shows a side-to-side rotation (driven by only the earthquake loading and the blade rotation) with a peak value of 0.09° for HP (Figure 6), which is 80% greater than that of the SS model (0.05°).

Referring to Figure 8, it is clear that at this stage, the SS model exhibited low plastic strain accumulation with nearly constant stiffness, as indicated by the green dashed line. In contrast, the HP model showed a much greater degradation in stiffness, represented by the blue dashed line, with a much lower slope compared to the dashed green line, accompanied by a continuous increase in plastic shear strain. However, by the end of this stage, the soil stiffness in the HP model partially recovered, as shown by the dotted blue line, which approached the slope of the green dashed line for the SS model.

Based on these observations, it may be concluded that during an earthquake, the foundation of the OWT exhibits a softer behavior with significantly greater accumulation of plastic shear strain in the HP model compared to the SS model.

3.1.3 Post-earthquake stage

In the post-earthquake stage, the structure shows a permanent tilting and a permanent lateral displacement in fore-aft and side-to-side directions for both soil models.

In the fore-aft direction (Figures 3 and 5), the HP model provides an average permanent rotation at mudline (calculated by averaging the time history during this stage) of 0.15° which is 56% greater than that of the SS model (0.096°), and an average permanent lateral displacement of 7.6 cm which is nearly 3 times greater than that of SS model (2.8 cm). In the side-to-side direction (Figures 4 and 6), the HP model provides an average permanent rotation value of 0.05° which is about 3 times greater than that of the SS model (0.016°). Moreover, HP provides a permeant lateral displacement in this direction equal to 3.7 cm, 3 times greater than that of SS (1.2 cm). These results are consistent with Figure 9, where both soil models exhibit the same stiffness (represented by the two green and blue dashed lines with nearly identical slopes) but with significantly greater plastic soil deformation in the HP model.

3.2 Tower top accelerations

Figures 10 and 11 show the time history of acceleration for the tower top in the fore-aft and vertical directions. For brevity, side-to-side acceleration was not shown as it follows the same trend as the fore-aft direction.

In the pre-earthquake stage and by neglecting the first 30 seconds (transitory behavior), the fore-aft acceleration time histories are nearly congruent for both SS and HP models (Figure 10) with a maximum value of about 1.12 m/s² for HP which is slighly higher than that of the SS (1 m/s²). This small difference aligns with the result found in section 3.1.1, where HP showed a nearly elastic behavior of foundation in fore-aft direction contrary to SS that showed an elasto-plastic one, thus leading to a lower fore-aft acceleration in presence of low-frequency vibration (wind and wave loading).

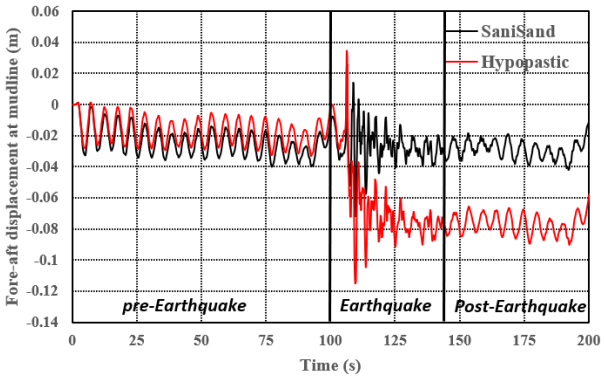

Figure 3. Fore-aft displacement of the monopile at mudline

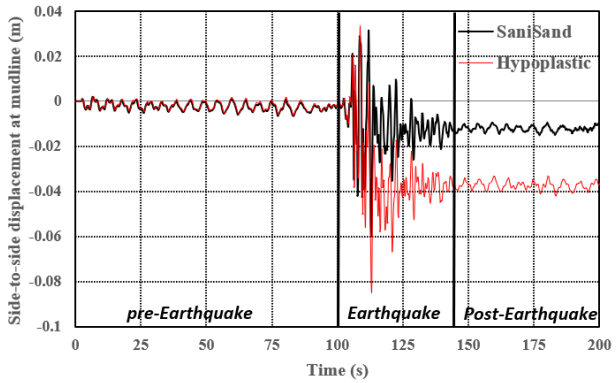

Figure 4. Side-to-side displacement of the monopile at mudline.

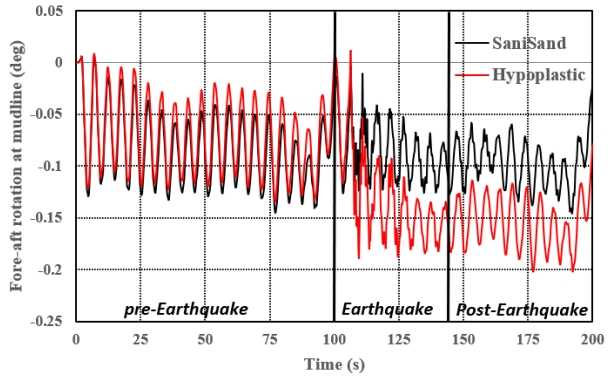

Figure 5. Fore-aft monopile rotation at mudline.

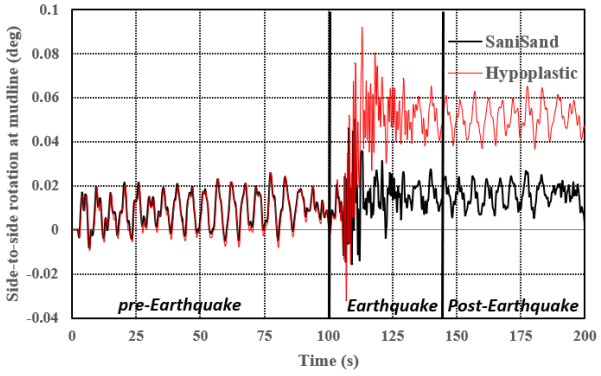

Figure 6. Side-to-side monopile rotation at mudline.

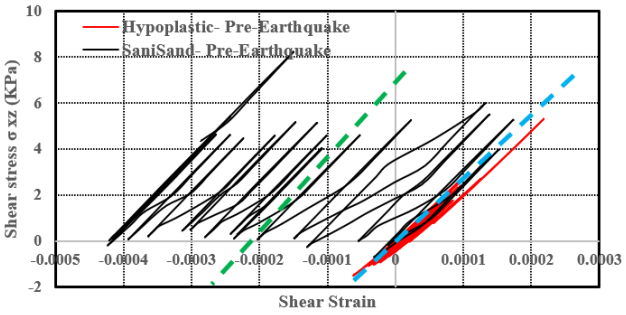

Figure 7. Shear stress - Shear strain behavior in xz plane during pre-earthquake stage.

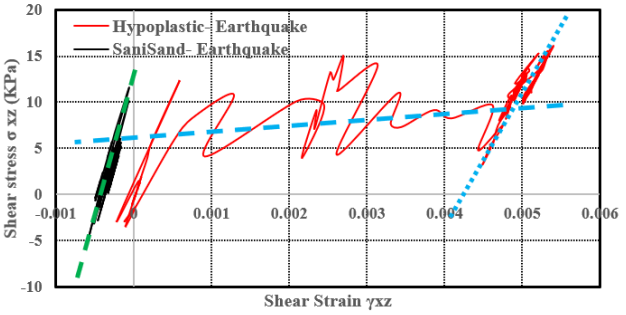

Figure 8. Shear stress - Shear strain behavior in xz plane during earthquake stage.

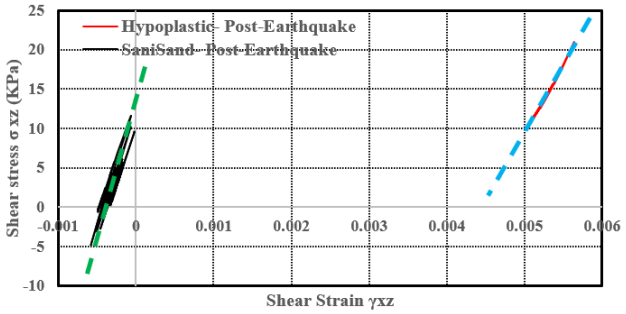

Figure 9. Shear stress - Shear strain behavior in xz plane during post-earthquake stage.

During the earthquake stage, SS exhibits a maximum fore-aft acceleration of 2.27 m/s² which is 35% higher than that of the HP model which reaches a maximum value of 1.68 m/s² (Figure 10). Additionally, SS shows a maximum vertical acceleration of 4 m/s² (Figure 11) which is about 2.5 times higher than that of the HP model (1.66 m/s²). These differences are attributed to the varying degrees of soil stiffness degradation shown in the two models during the earthquake (Figure 8), which leads to distinct shifts in the natural frequencies of the tower's fore-aft and vertical deformation modes. Consequently, the tower top experiences different acceleration responses depending on the frequency content of the applied seismic signal. In the post-earthquake stage, the fore-aft acceleration became identical for both soil models, with a maximum value of 0.75 m/s². This equality aligns with the close

stiffnesses (same slope for the green and blue dashed lines) of the soil observed in Figure 9.

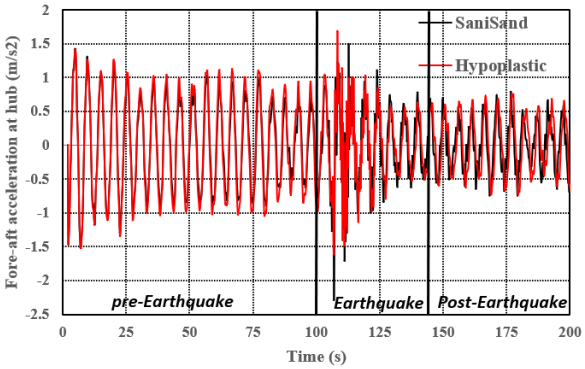

Figure 10. Fore-aft acceleration at tower top.

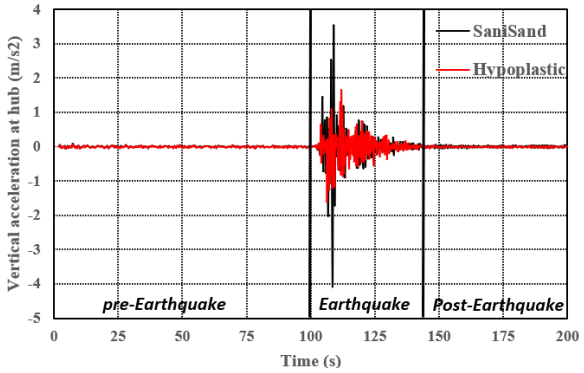

Figure 11. Vertical acceleration at tower top.

4 CONCLUSION

In this study, the responses of a DTU-10MW offshore wind turbine in terms of displacement and rotations at mudline and accelerations at tower top were computed and compared using the SaniSand and Hypoplastic soil models.

In the absence of an earthquake, the structural responses at mudline (displacements and rotations) were quasi-similar for both models. However, differences become evident under seismic and post-seismic conditions, where the HP model simulated a softer behavior of the soil compared to the SS model. After the earthquake, permanent displacement and tilting at mudline were more pronounced in the HP model than in the SS model.

Fore-aft and vertical acceleration at the tower top were higher in the SS model than in the HP model, during the earthquake. Based on the obtained results, it may be recommended, as a conservative approach in engineering practice, to use the hypoplastic model for determining displacements and rotations at the mudline, and the SaniSand model for the accelerations at tower top. These findings need to be verified through experimental tests to evaluate the accuracy of each soil model, and further numerical simulations for different seismic signals, and seismic parameters.

AUTHOR CONTRIBUTION STATEMENT

K. Dib: Data curation, Formal Analysis, Writing-Original draft. **Ph. Alkhoury**: Software support, Conceptualization, Methodology, Supervision. **A.-H. Soubra, F. Kaddah**: Conceptualization, Methodology, Supervision, Writing- Reviewing and Editing.

ACKNOWLEDGEMENTS

The authors are grateful for the financial support provided by “Conseil de recherche-Université Saint Joseph de Beirut”.

REFERENCES

API (2011). Petroleum and natural gas industries-specific requirement for offshore structures. Part 4-Geotechnical and foundation design considerations.

Alkhoury, Ph., Soubra, A.-H., Rey, V. and Aït-Ahmed, M. (2022). Dynamic analysis of a monopile-supported offshore wind turbine considering the soil-foundation-structure interaction. *Soil Dyn. & Earth. Engrg.*, 158.

Dafalias YF, Manzari MT. (2004). Simple plasticity sand model accounting for fabric change effects. *J Eng Mech*, 130(6):622–34.

Eslami, A. and Ghorbani, A. (2022). Seismic response of offshore wind turbines supported on monopiles and suction buckets: Numerical modelling and soft computing study. *Soil Dyn. & Earth. Engrg.*, 159.

Kuhlemeyer, RL., Lysmer, J. (1973). Finite element method accuracy for wave propagation problems. *J Soil Mech Found Div*, 99(5):421–7.

Niemunis, A. and Herle, I. (1997). Hypoplastic model for cohesionless soils with elastic strain range. *Mech Cohesive-Frict Mater*, 2: 279-299.

Totesten Whichman. (2016) https://www.torsten-wichtmann.de/

Wolffersdorff, P. A. V. (1996). A hypoplastic relation for granular materials with a predefined limit state surface. *Mech Cohesive-Frict Mater*, 1.

Zuo, H., Bi, K., Hao, H., Hong, H. and Li, Ch. (2019). Influence of earthquake ground motion modelling on the dynamic responses of offshore wind turbines. *Soil Dyn. & Earth. Engrg.*, 157.